Ionics (2015) 21:1391–1398
DOI 10.1007/s11581-014-1282-1

ORIGINAL PAPER

Almond shell-based activated nanoporous carbon electrode for EDLCs

Amrita Jain · S. K. Tripathi

Received: 19 March 2014 / Revised: 15 September 2014 / Accepted: 5 October 2014 / Published online: 18 October 2014

Abstract Almond shell-based chemically treated and activated nanoporous charcoal powder (AS(T)) has been successfully prepared by chemical activation method using potassium hydroxide (KOH) as an activating agent. The as-synthesized AS(T) was systematically characterized by various techniques like N_2 adsorption, scanning electron microscopy (SEM), X-ray diffraction, and thermogravimetric analysis. The AS(T)-based nanoporous activated charcoal is tested as an electrode material with ionic liquid-based polymer gel electrolyte for electrochemical double-layer capacitors (EDLCs). EDLCs prepared from AS(T) exhibit specific capacitance of 986.3 mF cm^{-2} (equivalent to single-electrode specific capacitance of 563.6 F g^{-1}). The energy density of 62.8 Wh kg^{-1} and power density of 2.1 kW kg^{-1} have been observed for nanoporous AS(T)-based EDLCs.

Keywords Almond shell · Nanoporous carbon · Ionic liquid · Electrochemical double-layer capacitor

Introduction

Supercapacitors, also called as ultracapacitors, are known as high power density output devices with high cyclic life [1]. Electrode materials are one of the dominating factors affecting the performance of supercapacitors. A wide range of carbon materials was successfully used as an electrode material for supercapacitors [2] due to their low cost, good electrical conductivity, and stable performance [3]. Various types of carbonaceous materials like carbon aerogels [4], carbon nanotubes [5], microporous carbon [6], hard-templated ordered mesoporous carbons [7, 8], and hierarchical porous carbons [9, 10] have been used as an electrode material for supercapacitors. But the method of preparation for such types of carbon requires expensive raw materials, a lot of time, energy, and complicated preparation procedures. In contrast, biomass wastes are very cheap and easily available, which make them potential raw materials for the preparation of porous carbons having good electrochemical capacitive performance.

Nowadays, much attention has been drawn towards utilization of biomass wastes to prepare porous carbon for electrochemical double-layer capacitors (EDLCs). Yang et al. [11] used walnut shells as precursors for the preparation of nanoporous carbon using physical–chemical activation simultaneously. They studied the pore structure, especially pore size distribution, of the resulting carbons and concluded that pore size distribution plays a significant role on the performance of EDLC. Raymundo-Piñero et al. [12] synthesized high-performance carbonaceous material for EDLCs using one-step carbonization of an oxygen-rich biopolymer. In their results, they concluded that the synthesized carbon has low specific surface area, but the capacitance value per unit mass of active material is comparable to the best activated carbon, which is due to the oxygen present in the carbon network participating in pseudo-faradic charge-transfer reactions. Guo et al. [13] synthesized porous carbon by chemical activation of rice husk. They found that the specific capacitance of the resulted carbons is not linearly proportional to the surface area but it strongly depends on the pore structure and functional groups of the carbon. Kim et al. [14] prepared activated carbon from bamboo waste by using chemical activation method. The prepared activated carbon with higher mesopore fraction gives higher capacitance in organic electrolyte and good rate capability in aqueous electrolyte.

A. Jain · S. K. Tripathi (✉)
Department of Physics, Jaypee University of Engineering and Technology, AB Road, Raghogarh, Guna, Madhya Pradesh 473226, India
e-mail: sktripathi16@yahoo.com

Almonds are one of the important stone fruits grown in India and are widely used throughout the country especially in winter season. The almond nutshells are waste materials and can be collected on community basis for reuse. Almond nutshells are abundant, inexpensive, and readily available waste lignocellulosic materials. In the present study, these nutshells were used to prepare activated carbon for its application as an electrode material in EDLCs.

In this work, we describe the synthesis technique of almond shell-based chemically treated and activated nanoporous charcoal powder (AS(T)) and its application as an electrode material in EDLC. The prepared activated charcoal was characterized using N_2 adsorption isotherm scanning electron microscopy (SEM), X-ray diffraction analysis (XRD), and thermogravimetric analysis (TGA). Further, an EDLC cell has also been fabricated using ionic liquid (IL)-based gel polymer electrolyte with AS(T) as an electrode material. Galvanostatic charge–discharge technique, ac impedance spectroscopy, and cyclic voltammetry (CV) test were used to characterize the EDLC cell.

Experimental details

Electrolyte optimization

The method of synthesis, optimization, and electrical characterization of poly(vinylidine fluoride-co-hexafluropropylene) (PVdF-HFP)–1-ethyl-2,3-dimethyl-imidazolium-tetrafluroborate [EDiMIM][BF_4]–propylene carbonate (PC)–magnesium perchlorate $Mg(ClO_4)_2$ was mentioned elsewhere [15].

Preparation of activated charcoal from almond shells

The almond shells were ground by pestle and mortar. For charcoal preparation, almond shells were kept in a muffle furnace at 300 °C for 5 h. This charcoal was soaked in a chemical solution of $CaCl_2$ (25 wt %) for 18–20 h to become activated charcoal. This activated charcoal was washed with double-distilled water. The samples were kept in oven at 110 °C (overnight) for drying. Further, chemical activation with potassium hydroxide (KOH) was carried out by using impregnation method. Five grams of activated charcoal was mixed by stirring a solution containing 15 ml of double-distilled water with activating agent KOH at 60 °C in 1:1 ratio. The resulting slurry was dried at 110 °C for 12–14 h. Then, the resulting mixture was used for carbonization. The carbonization was carried out in a muffle furnace, and the sample was heated (10 °C min^{-1}) from room temperature to the final carbonization temperature (T_{carb}=600 °C) in nitrogen atmosphere. The sample was kept at the final temperature for 1 h before cooling down up to room temperature under the same nitrogen flow. The pyrolyzed sample was washed repeatedly with HCl solution and later with double-distilled water until it gets free from chloride ions. Once the activating agent was removed, the sample was dried overnight.

Construction of electrodes

The electrodes were prepared by making a slurry of prepared activated charcoal powder and PVdF-HFP in the ratio 90:10 (*w*/*w*) in a common solvent acetone by thorough mixing. Fine films of electrodes were coated by spraying the slurry on carbon cloth (Ballard, USA) and kept in oven at 70 °C for 10–12 h.

Instrumental details

The microstructure and morphology of the almond shell-based treated activated charcoal powder were examined using scanning electron microscopy (SEM) with the help of JEOL Model-JSM 6380LA. Nitrogen adsorption–desorption isotherms were measured at 77 K using a Micrometrics Instruments Gemini Model 2380 analyzer after heating the sample at 100 °C for 2 h. The Brunauer–Emmett–Teller (BET) surface area of the samples was measured using nitrogen adsorption data over a relative pressure ranging from 0.05 to 1.0. X-ray diffraction (XRD) measurements were carried out using X'Pert PRO (PANalytical, Netherlands) using an operational voltage and current of 40 kV and 40 mA, respectively. In order to have a better understanding in the carbonization process, a thermogravimetric analyzer (Diamond TGA/DTA, Perkin Elmer Instruments, USA) was employed to monitor the volatile evolution behavior of EL(T) in N_2 atmosphere.

Electrochemical characterization

The EDLCs were fabricated using AS(T) electrodes with ionic liquid-based gel polymer electrolyte poly(vinylidine fluoride-co-hexafluropropylene) (PVdF-HFP)–1-ethyl-2,3-dimethyl-imidazolium-tetrafluroborate [EDiMIM][BF_4]–propylene carbonate (PC)–magnesium perchlorate $Mg(ClO_4)_2$ which was sandwiched between two symmetrical electrodes. The performance characteristics of the EDLCs were characterized by using ac impedance analysis, galvanostatic charge–discharge technique, cyclic voltammetry, and prolonged cyclic tests.

The ac impedance measurements for the characterization of EDLCs were carried out by using computer-controlled LCR HI TESTER (Model 3522-50, Hioki, Japan) in the frequency

range from 1 mHz to 100 kHz. The overall capacitance C of the capacitor cells was evaluated by using the relation

$$C = -1/\omega Z'' \tag{1}$$

where ω is the angular frequency and Z'' is the imaginary part of the total complex impedance. The single-electrode specific capacitance of the capacitor cells was evaluated by multiplying the overall capacitance by a factor of 2 and dividing by the mass of the single-electrode material.

The impedance data as a function of frequency were also analyzed by using the following equations:

$$C(\omega) = C'(\omega) - jC''(\omega) \tag{2}$$

where $C'(\omega)$ is the real part of complex capacitance and $C''(\omega)$ is the imaginary part of the complex capacitance $C(\omega)$. $C'(\omega)$ and $C''(\omega)$ are calculated by using the relations

$$C'(\omega) = -Z''(\omega)/\left\{\omega|Z(\omega)|^2\right\} \tag{3}$$

$$C''(\omega) = Z'(\omega)/\left\{\omega|Z(\omega)|^2\right\} \tag{4}$$

where $Z'(\omega)$ and $Z''(\omega)$ are, respectively, the real and imaginary parts of the complex impedance $Z(\omega)$ and ω is the angular frequency which is given by $\omega=2\pi f$.

The complex power of the fabricated cell was calculated by using the relation

$$S(\omega) = P(\omega) + jQ(\omega) \tag{5}$$

where $P(\omega)$ is the real part of the complex power which is also known as active power and $Q(\omega)$ is the imaginary part of the complex power and is also known as reactive power. $P(\omega)$ and $Q(\omega)$ are evaluated by using the following relations:

$$P(\omega) = \omega\, C''(\omega)\left|\Delta V_{\mathrm{rms}}\right|^2 \tag{6}$$

$$Q(\omega) = -\omega C'(\omega)\left|\Delta V_{\mathrm{rms}}\right|^2 \tag{7}$$

where $|\Delta V_{\mathrm{rms}}|^2=\Delta V_{\mathrm{max}}/\sqrt{2}$ with ΔV_{max} being the maximum amplitude of the ac signal.

The cyclic voltammetry was carried out by using computer-controlled CHI 608C (CH Instruments, USA). The capacitance values from this technique were evaluated by using the relation

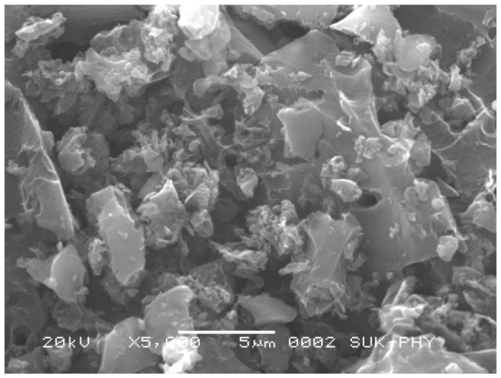

Fig. 1 SEM micrograph of AS(T) electrode

$$C = i/s \tag{8}$$

where i is the measure of constant current and s is the scan rate.

The charge–discharge characteristics of the capacitor cells were performed at a constant current, and their discharge capacitance C_{d} was calculated from the linear part of the discharge curves using the relation

$$C_{\mathrm{d}} = i\Delta t/\Delta V \tag{9}$$

where i is the constant current and Δt is the time interval for the voltage change ΔV.

Result and discussions

Textual characteristics of carbon materials

The morphology of the nanoporous AS(T) was observed by using scanning electron microscopy (SEM). The micrograph shows that AS(T) is heterogeneous in nature. The main feature of the synthesized AS(T) is the presence of compact aggregates of nanoporous carbon and graphitic carbon shells as shown in Fig. 1. Such type of morphology can be found as

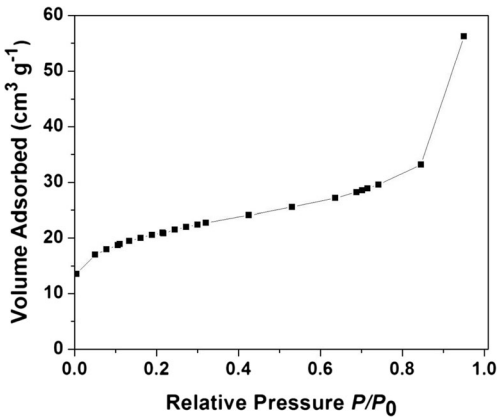

Fig. 2 Nitrogen adsorption isotherm of AS(T) at 77 K

Table 1 BET surface area and micropore volume of almond shell-based activated charcoal powder

Sample	BET surface area ($m^2\ g^{-1}$)	Micropore volume ($cm^3\ g^{-1}$)
AS(T)	214.4	0.038655

AS(T) almond shell-based chemically and treated activated charcoal

isolated aggregates or dispersed in an amorphous carbon matrix. Moreover, during chemical activation process, large mesopores in AS(T) are developed from small micropores through pore-widening effects. Although, the carbonization temperature is comparatively low, the presence of well-ordered nanometer-sized morphologies is an attractive as well as interesting textual characteristic of AS(T).

For double-layer formation, porosity of the carbon material is one of the most important parameters and is characterized by N_2 sorption at 77 K. The N_2 adsorption isotherm of nanoporous AS(T) is shown in Fig. 2. The isotherm of AS(T) can be classified as type I isotherm with a broad knee. It can be seen from the isotherm that uptake increases sharply at relative pressures ranging from 0.7 to 1.0, indicating the formation of very large mesopores and few macropores using KOH as an activating agent. This behavior also confirms the pore structure evolvement in double-layer formation. The BET surface area and micropore volume are enlisted in Table 1.

It should be pointed out that KOH (activating agent) plays a vital role in the development of pore structure. Upon KOH treatment, degradation of cellulose material and the aromatization of the carbon skeleton result in the creation of the porous structure. This enhancement in the formation of porous carbon from almond shells after the reaction with KOH may take place by the oxygen of the alkali which can eliminate the cross-linking and stabilizing of carbon atoms in crystallites. Potassium metal obtained at the reaction temperature may intercalate and force apart the separate lamellae of the crystallite. Eliminating potassium salts from the internal volume of the char by repetitive washing creates the porosity in this newly formed structure. Moreover, a further reaction between KOH and carbon formed at a previous stage may destroy the mesoporous structure and expand the pore volume of the carbon. The following reactions take place during the activation processes [16–18]:

$$4KOH + -CH_2 \rightarrow K_2CO_3 + K_2O + 3H_2$$
$$KOH + C \rightarrow 2K + CO$$
$$K_2CO_3 + 2C \rightarrow 2K + 3CO$$

KOH removes and avoids the cross-linking which helps in stabilizing the carbon atom in crystallites. Moreover, KOH acts as a dehydrating agent that encourages the decomposition of carbonaceous material during pyrolysis process which in turn restricts the formation of tar, thereby increasing the yield of mesoporous carbon.

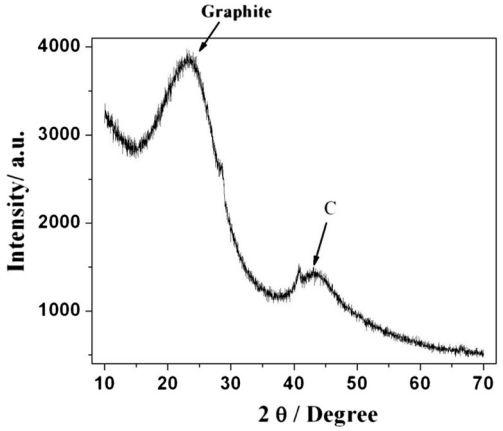

Fig. 3 XRD pattern of AS(T)

Figure 3 shows the XRD pattern of almond shell-based chemically treated activated charcoal. The XRD pattern of AS(T) shows a sharp peak at 2θ=24° and broad peak at 2θ= 42°. These peaks correspond to 100 and 002 planes which are generally observed for carbons. The Bragg angle at 24° corresponding to the diffuse scattering from disordered amorphous carbon shows a large full width and half maximum (FWHM) confirms the amorphous nature of synthesized carbon.

The temperature effect of the prepared activated charcoal was investigated by using thermogravimetric analysis (TGA). The mass loss of the material was calculated against the temperature rise. The TGA profile of AS(T) obtained under an inert gas condition is shown in Fig. 4.

The first weight loss of AST has been observed at 100 °C. This decrease in weight loss is probably due to thermodesorption of physically adsorbed material such as water vapor, hydrocarbon, etc. The second onset takes place at about 250 °C with a weight loss of about 33.5 % which implies that AS(T) becomes stable during pyrolysis with only 33.5 % remaining unburned or partially burned that may escape from AS(T) in the form of carbon dioxide and carbon monoxide at 600 °C. Hence, it can be concluded from TGA analysis that AS(T) is quite stable up to 800 °C.

Capacitive performance of AS(T) in ionic liquid-based polymer gel electrolyte EDLCs

The capacitor cell was constructed using AS(T) as an electrode material by sandwiching a polymer gel electrolyte in between them. So, the final configuration of the EDLC cell is

$$\text{Cell A}: \ \text{AS(T)}\big|\{\text{PVdF-HFP (70 wt\%)}\text{–}[\text{EDiMIM}][\text{BF}_4](30\ \text{wt\%})\}\{20\ \text{wt\%}\}\text{–}\{\text{PC-Mg}(\text{ClO}_4)_2(0.3\ \text{M})\}\{80\ \text{wt\%}\}\big|\text{AS(T)}.$$

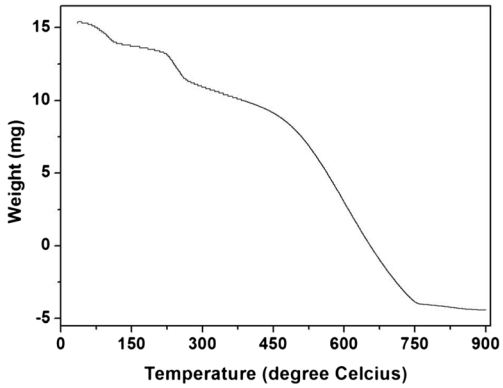

Fig. 4 Thermogravimetric analysis (TGA) plot of AS(T)

Figure 5 shows the cyclic voltammetry (CV) results for the AS(T)-based EDLC cell at different scan rates. The CV curves maintain a quite rectangular shape for EDLC cell A, indicating a reasonably good capacitive behavior with IL-based polymer gel electrolyte. As can be seen from Fig. 5, CV curves of cell A do not have any peaks, which indicates that supercapacitive behavior is free from redox reactions or is purely based on the electrostatic mechanism. Such type of pattern indicates the dominance of double-layer formation in the energy storage processes. Moreover, AS(T) mainly consists of mesopores, and this large pore size is expected to favor the fast electrolyte transport in the pore channel of AS(T). It has been shown that a larger pore size secures better capacitive performance in IL (for example, $EDiMIMBF_4$ in this case) which mainly consists of large ions and ion pairs. Therefore, it is hard for ions of IL to move in or out of micropores or small mesopores of carbon. The formation of an electrical double layer involves the ion transport in porous texture and the electrostatic adsorption of ions on the electrode/electrolyte interface. The effective area of ion-accessible electrode–electrolyte interface decides the performance of electrical double-layer capacitance. At a scan rate of 10 mV s^{-1}, AS(T) has a specific capacitance of 584.8 mF cm^{-2} (equivalent to single-electrode specific capacitance of 334.2 F g^{-1}), indicating that AS(T) has the largest accessible electrode/electrolyte interface area for the

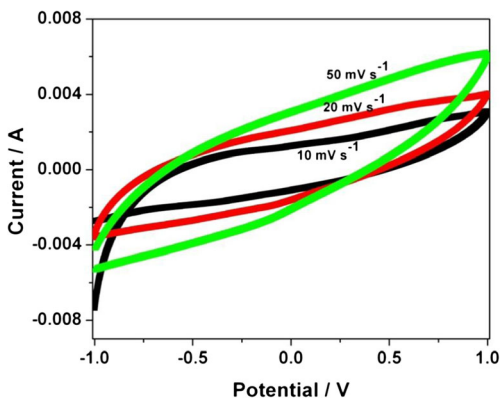

Fig. 5 Cyclic voltammograms of an EDLC cell AS(T)|PVdF-HFP–[EDiMIM][BF_4]–PC-Mg(ClO_4)$_2$|AS(T) at different scan rates

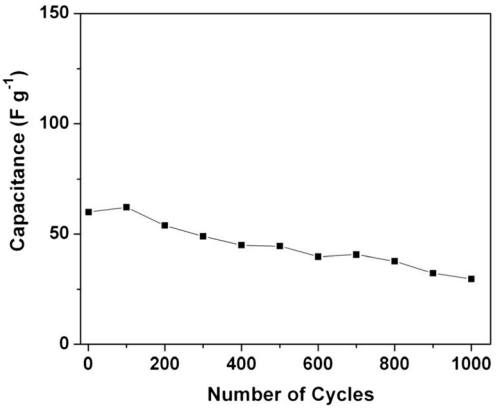

Fig. 6 Variation of capacitance of an EDLC cell, as a function of voltammetric cycles at a scan rate of 100 mV s^{-1}

$EDiMIMBF_4$ polymer electrolyte at this low scan rate. Therefore, it can be concluded that compatible to the pore size, the ion transport behavior is better in ionic liquid-based electrolytes. The capacitance values achieved in the present system might be due to the proper compatibility of the pore size of electrode materials with the ionic size of the ionic liquid-based polymer gel electrolytes. Cycling performance of the supercapacitor is very important in order to evaluate the electrochemical stability of the carbon material. Figure 6 shows the variation of specific capacitance as a function of cycle number. The capacitance was measured by using cyclic voltammetry at a scan rate of 100 mV s^{-1}. The result shows that specific capacitance decreased with increasing cycle numbers. After 1000 cycles of operation, the electrode can maintain ~85 % of the initial capacitance.

Electrochemical impedance spectroscopy is an important analytical technique which is used to get information about the frequency response of EDLCs and the capacitive phenomenon occurring at the electrode–electrolyte interface.

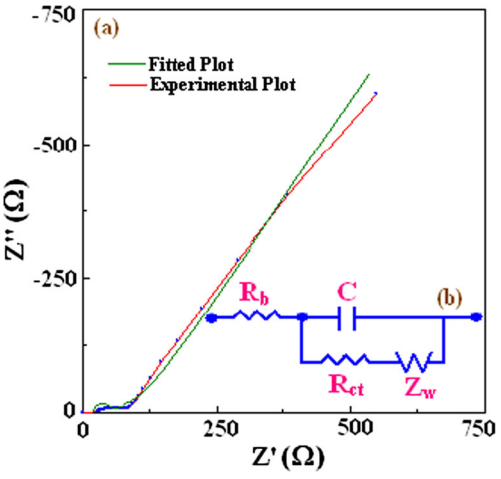

Fig. 7 (**a**) Electrochemical impedance spectra at 1 mHz of an EDLC cell AS(T)|PVdF-HFP–[EDiMIM][BF_4]–PC-Mg(ClO_4)$_2$|AS(T) [Experimental plot (red) and simulation plot (green)] at room temperature. (**b**) Equivalent circuit model

Table 2 Electrical parameters of an EDLC cell from impedance analysis

Cells	R_{ct} (Ω cm^{-2})	R_b (Ω cm^{-2})	10 mHz			1 mHz		
			R (Ω cm^{-2})	C		R (Ω cm^{-2})	C	
				(mF cm^{-2})[a]	(F g^{-1})[b]		(mF cm^{-2})[a]	(F g^{-1})[b]
A	9.83	5.61	35.8	355.4	203.1	109.4	986.3	563.6

[a] Overall capacitance of the cell

[b] Single-electrode specific capacitance of the cell

Figure 7(a) shows the Nyquist plot of the EDLC cell A. As can be seen from the impedance plot, a typical feature of a porous electrode has been observed in the Warburg region at medium frequencies and straight line at low frequencies. At low frequencies, the plot assumes the shape close to that of an ideal capacitor. The AS(T)-based EDLC cell shows a semicircle at mid-high frequencies which may be due to the diffusion process of the ions of electrolyte into the pore channels of the carbons. At high frequencies, the resistance characteristics of an EDLC cell are given by equivalent series resistance (ESR) which includes the electrolyte resistance, the collector–electrode contact resistance, and the electrode–electrolyte interface resistance. The values of bulk resistance R_b and charge transfer resistance R_{ct} as calculated from the intercepts of the real axis of the complex impedance response, along with the total resistance R and capacitance C, are summarized in Table 2.

In order to gather quantitative electrochemical impedance spectroscopy (EIS) information about the AS(T)-based electrode material, an equivalent circuit model representing the electrostatic charge storage mechanism at the electrode–electrolyte interface in the potential range of interest is shown in Fig. 7(b). The analysis of $Z(\omega)$ is carried out by using the following equations:

$$Z(\omega) = R_b + Z_1(\omega) \tag{10}$$

$$\frac{1}{Z_1(\omega)} = \frac{1}{R_{ct} + ZW} + j\omega C_{dl} \tag{11}$$

where ω, R_b, Z_1, Z_W, R_{ct}, and C_{dl} are the angular frequency, bulk electrolyte resistance, impedance of AS(T)/electrolyte interface, Warburg diffusion impedance, charge transfer

Table 3 The best fitting values of the equivalent circuit elements of Fig. 7(b) for the impedance data shown in Fig. 7(a)

Parameters	AS(T)
R_b (Ω cm^{-2})	4.0
R_{ct} (Ω cm^{-2})	5.8
C_{dl} (μF cm^{-2})	3.88
α	0.3

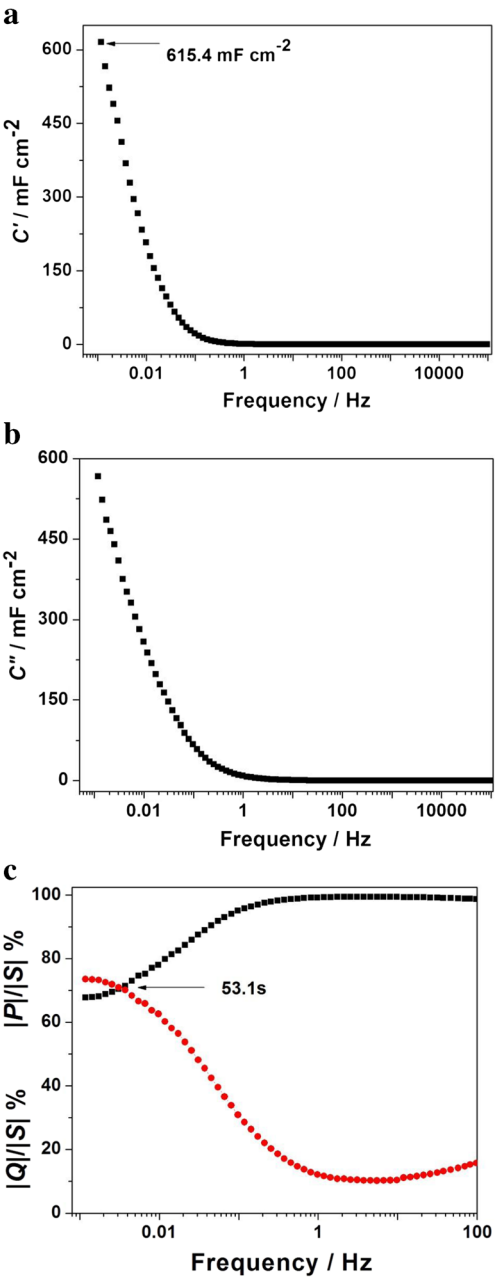

Fig. 8 Bode plots for **a** real part and **b** imaginary part of capacitance as a function of frequency. **c** Plot of normalized active power $|P|/|S|$ and reactive power $|Q|/|S|$ as a function of frequency (in logarithmic scale)

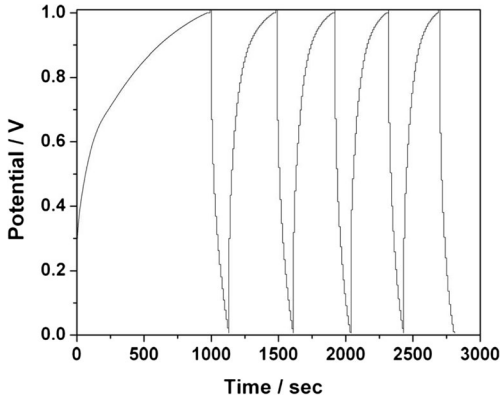

Fig. 9 Charge–discharge curve of EDLC cell AS(T)|PVdF-HFP–[EDiMIM][BF_4]–PC-Mg(ClO_4)$_2$|AS(T) at a current density of 5.0 mA cm^{-2}

resistance at the AS(T)/electrolyte interface, and double-layer capacitance, respectively.

Based on the EIS spectra in Fig. 7(a), the best fit values of the equivalent circuit are shown in Fig. 7(b) and are enlisted in Table 3. The green line in Fig. 7(a) shows the best fit spectra, which almost overlaps with the experimental curve and hence indicates the good fitting of the experimental data. From Table 3, the low values of bulk resistance R_b of the electrolyte material are attributed to the presence of ionic liquid which shows a liquid-like conductivity mechanism of the polymer gel electrolyte and in turn improves the overall device performance. Further, the value of charge transfer resistance (R_{ct}) is also low, suggesting the better pore accessibility of AS(T) electrodes to the ions of electrolyte material, and hence, higher capacitance values are achieved. This statement is further supported by the lower resistance values obtained for Warburg element which gives the idea of ion diffusion into the bulk of the electrode. Combining all the tabulated results, it can be inferred that lower values of bulk resistance, charge transfer resistance, and Warburg element are a typical merit of almond shell-based activated charcoal as an electrode material for EDLCs having high specific capacitance and excellent power ability.

Figure 8a, b represents the Bode plots of the real ($C'(\omega)$) and imaginary ($C''(\omega)$) parts of the complex capacitance ($C(\omega)$) as a function of frequency. It gives an in-depth look of the electrochemical properties of EDLCs. At low frequency, $C'(\omega)$ represents the capacitance of the electrode material and $C''(\omega)$ corresponds to the energy dissipation by an irreversible process that represents the hysteresis of the materials [19]. It has been observed from Fig. 8a that at lower frequency (i.e., at 1 mHz), the capacitance value is found to be of the order of 615.4 mF cm^{-2} for AS(T)-based EDLC. As frequency increases, the capacitance shows a frequency-dependent behavior and $C'(\omega)$ drops sharply in between the frequency range of 10 and 60 mHz. At higher frequency, the capacitance is insignificant and the EDLC cell behaves like a pure resistor. The imaginary part of the capacitance $C''(\omega)$ with frequency is given in Fig. 8b. As per convention, the maximum point of the curve represents the complete system, which describes the transition point at which the circuit changes its behavior from a purely resistive to a purely capacitive character [20].

The plots of $|P|/|S|$ and $|Q|/|S|$ of the complex power vs. frequency (expressed in logarithmic scale) for cell A are shown in Fig. 8c. The power dissipated into the system can be calculated from the normalized active power which is denoted by $|P|/|S|$. At high frequency, when the supercapacitor behaves like a pure resistor, all the power is dissipated into the system (P=100 %); on the other hand, at low frequency, no power is dissipated into a pure capacitance. The intersection of two plots occurs at frequency f_0, which is also known as resonance frequency with the help of which relaxation time constant τ_0 ($=2\pi f_0$) can be determined explicitly. From the crossing of two plots at a frequency f_0, the value of τ_0 has been calculated. The calculated relaxation time constant τ_0 for cell A is 53.1 s, which lies within the same order of magnitude as reported by some other workers [21].

The galvanostatic charge–discharge curves for the AS(T)-based EDLC are recorded in the potential range of 0–1.0 V at a current density of 5 mA cm^{-2} and are shown in Fig. 9. As can be seen from Fig. 9, the EDLC cell shows a similar symmetrical triangular curve with a nearly linear variation of voltage as a function of time during charge and discharge. Such type of curve is typical for carbon-based EDLC, and hence, it confirms that EDLC cell A has good capacitive performance [22, 23]. Further, as can be seen from Fig. 9, EDLC cell A shows significantly higher charge–discharge times, which indicates that a large number of electrons and electrolyte ions are participating in the charging and discharging process of AS(T)-based electrodes. From Fig. 9, it has also been observed that there is an initial sudden voltage drop during the

Table 4 Typical charge–discharge characteristics of an EDLC cell at a current density of 5.0 mA cm^{-2}

Cells	R_i (Ω cm^{-2})	Discharge capacitance, C_d		Working voltage (V)	Energy density (Wh kg^{-1})	Power density (kW kg^{-1})
		(mF cm^{-2})[a]	(F g^{-1})[b]			
A	73.3	790.9	451.9	1.0	62.76	2.1

[a] Overall capacitance of the cell

[b] Single-electrode specific capacitance of the cell

discharging process which may be due to the diffusion-limited mobility of the electrolyte ions in the electrode pores. This limitation is associated with the equivalent series resistance (ESR) of EDLC cell A. The discharge capacitance C_d values have been calculated from the linear part of the discharge characteristics using Eq. (9). The values of internal resistance R_i and discharge capacitance C_d of EDLC cell A are listed in Table 4.

Conclusions

Almond shell-based chemically treated and activated nanoporous charcoal powder having a specific surface area of 214.4 $m^2\ g^{-1}$ was successfully synthesized using KOH as an activating agent. Electrochemical studies show that AS(T) electrode-based EDLCs show excellent capacitive behavior in IL-based electrolyte having a specific capacitance of 986.3 mF cm^{-2} (equivalent to a single-electrode specific capacitance of 563.6 F g^{-1}). The EDLC cell shows almost stable capacitance values up to 1000 cycles and even more. The energy density of 62.8 Wh kg^{-1} and power density of 2.1 kW kg^{-1} have been achieved for nanoporous AS(T)-based EDLCs. This findings draw attention towards the possibility of a low-cost biomass-based electrode material for ionic liquid-based electrochemical double-layer capacitors.

Acknowledgments The authors are grateful to the Madhya Pradesh Council of Science and Technology, Madhya Pradesh, India, for providing financial support through Grant-in-Aid for Scientific Research vide sanction no. 3683/CST/R&D/Phy & Engg. Sc/2012, Bhopal (dated: 03.11.2012). The authors are also thankful to Rakesh Srivastava, HEG, India; Dr. S.A. Hashmi, University of Delhi, India; and Dr. O.P. Modi, AMPRI, India, for providing SEM, BET, TGA, and XRD results.

References

1. Conway BE (1999) Electrochemical supercapacitors: scientific fundamentals and technical applications. Kluwer Academic/Plenum Publishers, New York
2. Chmiola J, Largeot C, Taberna PL, Simon P, Gogotsi Y (2010) Science 328:480–483
3. Kötz R, Carlen M (2000) Electrochim Acta 45:2483–2489
4. Li W, Probstle H, Fricke J (2003) J Non-Cryst Solids 325:1–5
5. Dong B, He BL, Xu CL et al (2007) Mat Sci Eng B 143:7–13
6. Chmiola J, Yushin G, Gogotsi Y et al (2006) Science 313:1760–1763
7. Wang DW, Li F, Liu M et al (2007) New Carbon Materials 22:307–314
8. Zhang FQ, Meng Y, Gu D et al (2006) Chem Mater 18:5279–5288
9. Wang DW, Li F, Liu M et al (2008) Angew Chem Int Ed 47:373–376
10. Xing W, Huang CC, Zhuo SP et al (2009) Carbon 47:1715–1722
11. Yang J, Liu Y, Chen X et al (2008) Acta Phys-Chim Sin 24:13–19
12. Raymundo-Piñero E, Leroux F, Béguin F (2006) Adv Mater 18:1877–1882
13. Guo Y, Qi J, Jiang Y et al (2003) Mater Chem Phys 80:704–709
14. Kim YJ, Lee BJ, Suezaki H et al (2006) Carbon 44:1592–1595
15. Amrita J, Tripathi SK, Ashish G, Manju M (2013) J Solid State Electrochem 17:713–726
16. Wu FC, Tseng RL, Hu CC, Wang CC (2005) J Power Sources 144:302–309
17. Cao Q, Xie KC, Lv YK, Bao WR (2006) Bioresour Technol 97:110–115
18. Chunlan L, Shaoping X, Yixiong G, Shuqin L, Changhou L (2005) Carbon 43:2295–2301
19. Taberna PL, Simon P, Fauvarque JF (2003) J Electrochem Soc 150:A292–A300
20. Wang J, Chen M, Wang C, Wang J, Zheng J (2011) J Power Sources 196:550–558
21. Farma R, Deraman M, Talib IA et al (2013) Int J Electrochem Sci 8:257–273
22. Jena A et al (2012) J Electrochem Soc 159:1682–1689
23. Mosqueda HA et al (2010) Electrochim Acta 55:7479–7483